Supplementary Information

Covalent organic frameworks with spatially separated triad architecture for sacrificial agent–free H_2O_2 photosynthesis

Jing-Yi Li, Xiu Wang, Wei-Rong Cui*

College of Chemistry and Materials, Gannan Normal University, Ganzhou 341000, China

E-mail: wrcui@gnnu.edu.cn.

1. Experiment Details

1.1 Materials

Benzo[c][1,2,5]thiadiazole-4,7-dicarbaldehyde (TzA), 2,5-di(thiophen-2-yl)terephthalaldehyde (TpA) and 2,4,6-trimethyl-1,3,5-triazine (TMT) were purchased from Shanghai Tensus Bio-tech Co., Ltd. Sodium ethoxide (EtONa), KOH, $AgNO_3$, *p*-benzoquinone (*p*-BQ), L-histidine, and KI were purchased from Energy Chemical Technology (Shanghai) Co., Ltd. Solvents including trifluoroacetic acid, methanol (MeOH), pyridine, isopropanol (IPA) and 1,8-diazabicyclo[5.4.0]undec-7-ene (DBU) were purchased from Energy Chemical Technology (Shanghai) Co., Ltd.

1.2 Characterization

Powder X-ray diffraction (PXRD) patterns of the monomers and resulting COFs were acquired on a Bruker AXS D8 Advance A25 Powder X-ray diffractometer (40 kV, 40 mA) using Cu Kα (λ=1.5406 Å) radiation. Fourier-transform infrared (FT-IR) spectra were recorded on a Nicolet iS50 FT-IR spectrometer. X-ray photoelectron spectroscopy (XPS) was performed on ground powders using a Thermo VG Multilab 2000X. The test Passing-Energy full spectrum is 50 eV, the narrow spectrum is 20 eV, the step length is 0.05 eV, the residence time is 40-50 ms, and the charge correction is carried out with C 1s=284.80 eV binding energy as the energy standard. The morphology of the material was imaged by a scanning electron microscope (SEM, JEM-2010, JEOL). Solid-state ^{13}C cross-polarization magic-angle spinning (CP/MAS) NMR spectra were obtained using a 4-mm double-resonance MAS probe with a spinning rate of 10.0 kHz, a contact time of 2 ms (ramp 100), and a pulse delay of 3 s. Prior to porosity analysis, samples were degassed at 120 °C for 12 h. Nitrogen adsorption–desorption isotherms were measured at 77 K on a Micromeritics ASAP 2020M system. The Brunauer–Emmett–Teller (BET) method was applied to calculate the specific surface areas, and pore size distributions were derived using non-local density functional theory (NLDFT). Thermogravimetric analysis (TGA) was conducted on a Linseis STA PT1600 instrument under a nitrogen atmosphere, heating from 30 to 800 °C at a rate of 10 °C min^{-1}. UV–vis diffuse reflectance spectra (DRS) were recorded

at room temperature on a PerkinElmer Lambda 900 spectrophotometer. Electron paramagnetic resonance (EPR) spectra were collected at room temperature using a Bruker EMX PLUS spectrometer. In situ diffuse reflectance infrared Fourier transform spectroscopy (DRIFTS) was performed on a Bruker INVENIO R FT-IR spectrometer equipped with a Harrick in situ diffuse reflectance cell. The apparent quantum yield (AQY) was calculated by a 300 W Xenon lamp (Beijing China Education Au-Light Co. Ltd., CEL-HXF300-S) and optical radiometer (Beijing China Education Au-Light Co. Ltd., CEL-NP2000-2(10)A).

1.3 Photocatalytic H_2O_2 production

COFs (TpA-TzA、TpA-TMT and TzA-TMT, 2 mg) and water (20 mL) were put in a quartz reactor. To ensure uniform dispersion of the photocatalyst, the suspension was well dispersed by sonicating for 30 min. Subsequently, the mixture was thoroughly degassed by bubbling oxygen (O_2) for 30 min. Prior to irradiation, the solution was stirred for 30 min under dark conditions to establish adsorption-desorption equilibrium. The reaction mixture was then illuminated using the light source: a 300 W Xenon lamp. Throughout the reaction, the temperature of the entire system was maintained at 25 °C. After sampling every 15 min, the H_2O_2 content in the solution was detected after the catalyst was filtered.

1.4 H_2O_2 detection methods

The amount of H_2O_2 was analyzed by iodometry. 1 mL of 0.1 mol·L^{-1} $C_8H_5KO_4$ aqueous solution and 1 mL of 0.4 mol L^{-1} KI aqueous solution were added to the obtained solution (0.5 mL), which was then kept for 30 min. H_2O_2 molecules react with iodine ions (I^-) under acidic conditions to generate triiodide ions (I_3^-) (followed as the reaction equation $H_2O_2 + 3I^- + 2H^+ \rightarrow I_3^- + 2H_2O$), which have strong absorption near 352 nm. The absorbance of I_3^- at 352 nm was measured by an ultraviolet spectrophotometer, and then the amount of H_2O_2 generated by each reaction can be calculated by equation $c(H_2O_2) = c(I_3^-)$.

The standard curve diagram is as follows:

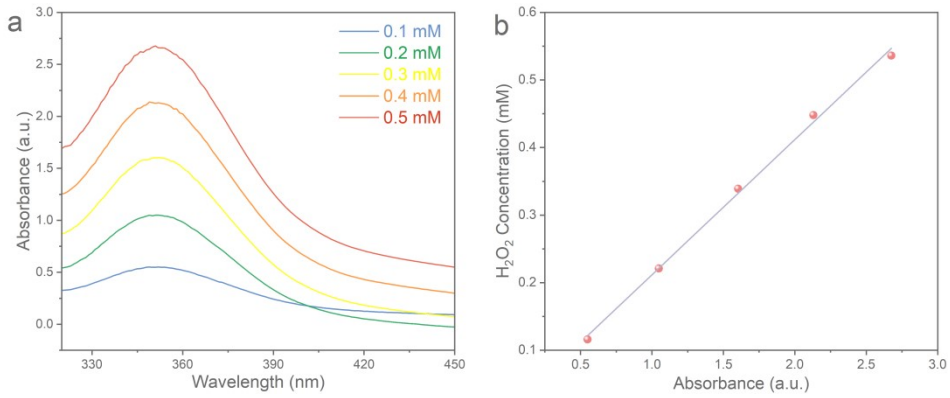

1.5 Calculation methods

Geometry optimisations were performed using Gaussian 16, employing the B3LYP functional and 6-31G(d) basis set. The geometry optimisations were run with dispersion corrections from Grimme's D3 model with Becke-Johnson damping factors. Harmonic vibrational frequencies calculations were performed to confirm the stationary points as true minima. The single point energies and frequencies are calculated using the B3LYP functional and the 6- 311g (d,p) basis set.

For the analysis of excited state electron and hole analysis, centroid D index of holes and electrons, Chole and Cele plots, contribution values of excited state electrons, all of which are extracted by Multiwfn wave function analysis software and analyzed and plotted by VMD software. TD-DFT method and CAM-B3LYP method are used to calculate the excited states of molecules. The adsorption energy is calculated by subtracting the energy of adsorbent and the energy of adsorbate from the energy of adsorption complex. The ball and stick structures were created using GaussView 6.1.1.

1.7 Synthesis of COFs

Synthesis of TpA-TzA: Benzo[c][1,2,5]thiadiazole-4,7-dicarbaldehyde (TzA) (28.83 mg, 0.15 mmol), 2,5-di(thiophen-2-yl)terephthalaldehyde (TpA) (44.76 mg, 0.15 mmol), 2,4,6-trimethyl-1,3,5-triazine (TMT) (24.63 mg, 0.20 mmol) and KOH (33.66 mg, 0.6 mmol) were dissolved in a mixed solvent containing 2.8 mL *n*-Butanol and 1.2 mL 1,2-dichlorobenzene; Subsequently, the resulting pale-yellow solution was heated at 120 ℃ for 3 days. After cooling to room temperature, the precipitate was collected

and washed with methanol, tetrahydrofuran, acetone and dichloromethane in sequence for three times (10 mL for each), and then dried under vacuum at 120 °C for 12 h. Finally, pure COF sample was afforded as yellow powder.

Synthesis of TpA-TMT: 2,5-Di(thiophen-2-yl)terephthalaldehyde (TpA) (89.52 mg, 0.30 mmol), 2,4,6-trimethyl-1,3,5-triazine (TMT) (24.63 mg, 0.20 mmol) and KOH (33.66 mg, 0.6 mmol) were dissolved in a mixed solvent containing 2.8 mL *n*-Butanol and 1.2 mL 1,2-dichlorobenzene; Subsequently, the resulting pale-yellow solution was heated at 120 ℃ for 3 days. After cooling to room temperature, the precipitate was collected and washed with methanol, tetrahydrofuran, acetone and dichloromethane in sequence for three times (10 mL for each), and then dried under vacuum at 120 °C for 12 h. Finally, pure COF sample was afforded as orange powder.

Synthesis of TzA-TMT: Benzo[c][1,2,5]thiadiazole-4,7-dicarbaldehyde (TzA) (57.66 mg, 0.3 mmol), 2,4,6-trimethyl-1,3,5-triazine (TMT) (24.63 mg, 0.20 mmol) and KOH (33.66 mg, 0.6 mmol) were dissolved in a mixed solvent containing 2.8 mL *n*-Butanol and 1.2 mL 1,2-dichlorobenzene; Subsequently, the resulting pale-yellow solution was heated at 120 ℃ for 3 days. After cooling to room temperature, the precipitate was collected and washed with methanol, tetrahydrofuran, acetone and dichloromethane in sequence for three times (10 mL for each), and then dried under vacuum at 120 °C for 12 h. Finally, pure COF sample was afforded as yellow green powder.

1.8 Control experiments

To investigate the reaction mechanism and intermediates, photocatalytic H_2O_2 reactions were performed under different conditions and with different sacrificial reagents. 2 mg catalyst was added to methanol (MeOH, h^+ scavenger, 10%) with O_2-bubbling, $AgNO_3$ (e^- scavenger, 1 mM) under O_2 atmosphere, $AgNO_3$ (e^- scavenger, 1 mM) under N_2 atmosphere, isopropanol (IPA, hydroxyl radical scavenger, 10%) with O_2-bubbling, L-histidine (Singlet oxygen radical scavenger, 1mM) with O_2-bubbling or *p*-benzoquinone (*p*-BQ, superoxide radical scavenger, 1 mM) with O_2-bubbling, respectively, to conduct control experiments.

1.9 Cycling tests

After the reaction, the polymer photocatalyst was centrifuged, washed with methanol, and dried in a vacuum oven at 80 °C for 12 h. The resulting photocatalyst was then directly used for the subsequent runs.

1.10 Reaction condition optimization

In order to synthesize TpA-TzA with high crystallinity, we have optimized the reaction condition by changing the solvents, catalysts, concentrations of catalyst and temperatures. After many different trials, we successfully get the right condition to obtain high crystallinity TpA-TzA COF.

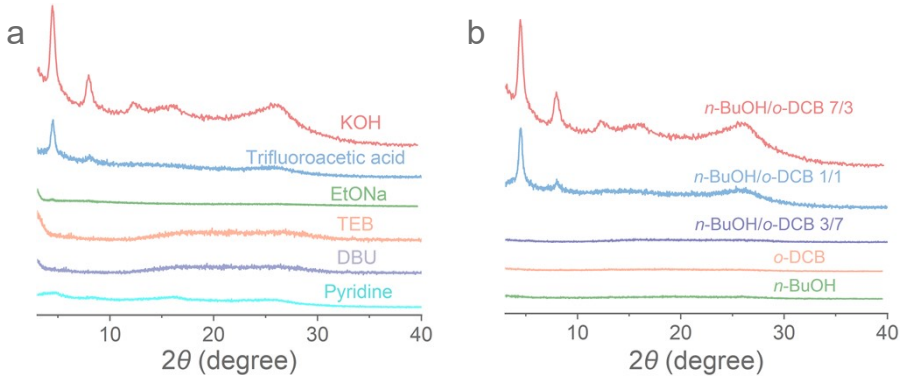

Figure S1. PXRD patterns of attempts to synthesize TpA-TzA under different reaction conditions.

1.11 Electrochemical measurements

A three-electrode cell was utilized to measure the transient photocurrent responses (I-t), electrochemical impedance spectra (EIS), and Mott-Schottky (M-S) plots on an IVIUM Vertex. C EIS electrochemical workstation. Prior to any measurements, the working electrodes were immersed in the electrolyte for 60 s. The supporting electrolyte was a 0.1 M Na_2SO_4 aqueous solution, and the light source was a 300 W Xe-lamp equipped with a cutoff filter ($\lambda \geq 400$ nm). A platinum plate served as the counter electrode, and a saturated Ag/AgCl electrode was used as the reference electrode. The potential of the Ag/AgCl electrode was converted to the reversible hydrogen electrode (RHE) using the following expression: $E_{RHE} = E_{Ag/AgCl} + 0.0591pH + E^{\theta}_{Ag/AgCl}$ ($E^{\theta}_{Ag/AgCl}$=0.199 V).

The preparation process of the working electrodes is as described below. Firstly, indium-tin oxide (ITO) glasses were sonicated in acetone, ethanol, and ultra-pure water successively for 30 min each and then dried under a nitrogen flow. Next, 5 mg of COF was combined with 20 μL of a 5% Nafion aqueous solution and 0.5 mL of ethanol, and sonicated for 30 min to form a slurry. Subsequently, 50 μL of this slurry was spread onto an ITO glass with an area of 1×1 cm^2 and a resistance of 2 Ω. After drying with nitrogen, the boundary of the electrode was isolated using epoxy resin. The photocurrent intensity of as-prepared electrodes is measured at 0 V versus Ag/AgCl with the light on and off. EIS is determined over the frequency range of 102-106 Hz with an ac amplitude of 10 mV at the open circuit voltage under room-light illumination. A mixed solution of KCl, $K_3Fe(CN)_6$, and $K_4Fe(CN)_6 \cdot 3H_2O$ (pH=5, 0.1 mol L^{-1}) was employed as the electrolyte in the EIS measurements.

1.12 Electrochemical rotating ring-disk electrode (RRDE) measurement

The RRDE performance was tested using a CS2350H electrochemical analyzer and a pine-modulated speed rotator. In particular, the RRDE electrode (surface: 0.2475 cm^2) was selected as the working electrode, with a Pt plate as the counter electrode, and a saturated Ag/AgCl as the reference electrode. The working electrode was prepared as follows: the catalyst ink was prepared by ultrasonic dispersion of 4 mg polymer in 400 μL mixture solution (380 μL ethanol and 20 μL 5% Nafion), and then 15 μL catalyst ink was drop-added to the electrode surface to form a catalyst film after 1 hour of natural air drying. The ORR polarization curves were collected by linear sweep voltammetry (LSV) in an O_2-saturated 0.1 M phosphate buffer solution (pH=7.2) with a sweep rate of 10 mV s^{-1} at 900 rpm. The transfer number of electrons (n) was calculated by the disk current (I_d) and ring current (I_r) results as per the following equations:

$$n = 4 \times \frac{I_d}{I_d + {I_r}/{N}}$$

$$H_2O_2 = 200 \times \frac{I_r/N}{I_d + I_r/N}$$

Here, I_d and I_r represent the disk and ring currents (mA), respectively, and N is the collection efficiency of the Pt ring (N = 0.37).

1.13 Structural modelling and Pawley refinement

Structural Modeling and Pawley Refinement Structural modeling of the TpA-TzA, TpA-TMT, and TzA-TMT complexes was performed using the MATERIAL Studio suite to obtain packing models and their corresponding unit cells. All the alternative, eclipsed, slipped and staggered stacking models were constructed and optimized with the Forcite module. The space group with the highest symmetry was selected to simulate the XRD pattern and compare with the experimental results. Pawley refinement was applied to define and optimize the lattice cell parameters.

1.14 Apparent quantum yield (AQY) measurements

The AQY for H_2O_2 was measured under the irradiation of a 300W Xenon lamp equipped with different bandpass filters (400, 460, 520, 578 and 620 nm). After ultrasonication and O_2 bubbling, the photocatalytic reaction was conducted in pure water (20 mL) with photocatalyst (20 mg) at 25 °C. The AQY is calculated by the following equation:

$$AQY(\%) = \frac{2n_{H_2O_2}}{n_{photon}} \times 100\%$$

$$n_{photon} = \frac{E_{total}}{E_{photon}} = \frac{ISt}{N_A hc/\lambda}$$

where n_{H2O2} is the amount of H_2O_2 generated (mol), n_{photon} is the photon number entered into the photoreactor (mol), N_A is Avogadro constant, h is the Planck constant, c is the speed of light, S is the irradiation area (19.625 cm^2), I is the intensity of irradiation light, t is the photoreaction time, λ is the wavelength of the monochromatic light (nm).

1.15 The solar-to-chemical energy conversion (SCC)measurements

The 20 mg catalyst was well dispersed in 20 mL deionized water and degassed by O_2 bubbling for 30 min before being sealed in vessel. A Xenon solar simulator was used as the light source (AM 1.5G, 100 mW cm^{-2}). The reaction temperature was kept at 25°C. The SCC efficiency was calculated via the following equation:

$$SCC(\%) = \frac{[\Delta G\ for\ H_2O_2\ generation(\frac{J}{mol}) \times [H_2O_2\ produced(mol)}{[total\ input\ energy(W)] \times [reaction\ times(s)]} \times 100\%$$

Where, the free energy (ΔG) for H_2O_2 formation is 117 kJ mol^{-1}, the irradiance of the spectrum is 1000 W m^{-2} and the irradiated area is 19.625 cm^2.

1.16 Photocatalytic evolution of $\cdot O_2^-$

The quantitative analysis of $\cdot O_2^-$ was performed using a nitro blue tetrazolium (NBT) assay, and the calculation procedure has now been clarified as follows:NBT can be reduced by $\cdot O_2^-$ to form insoluble formazan. In this work, NBT (0.1 mM) was dispersed in PBS (pH = 7), and COF samples were added into 5 mL of this solution. After irradiation under a 300 W Xe lamp, the suspension was filtered and the filtrate was analyzed by UV-vis spectroscopy. Allowing the concentration of residual NBT to be determined from the absorbance at 260 nm. The consumption of NBT was calculated according to:

$$C_{NBT} = C_0 - C_t$$

where C_0 and C_t represent the initial and remaining concentrations of NBT, respectively.Based on the reaction stoichiometry (NBT : $\cdot O_2^-$ = 1 : 4, as shown in the reaction equation)

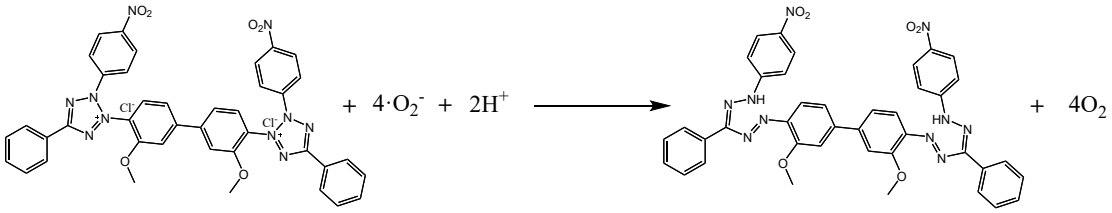

The concentration of generated $\cdot O_2^-$ was calculated using: $C_{\cdot O_2^-} = 4 \times C_{NBT}$

Therefore, the amount of $\cdot O_2^-$ produced was quantified by monitoring the decrease in NBT concentration over time.

2. Supplementary Data

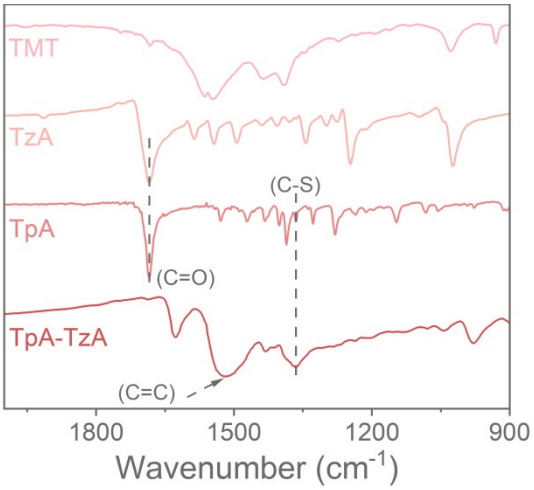

Figure S2. FTIR spectra of TpA-TzA.

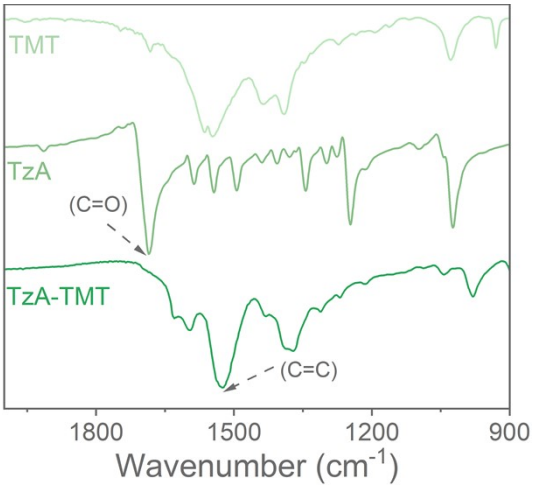

Figure S3. FTIR spectra of TzA-TMT.

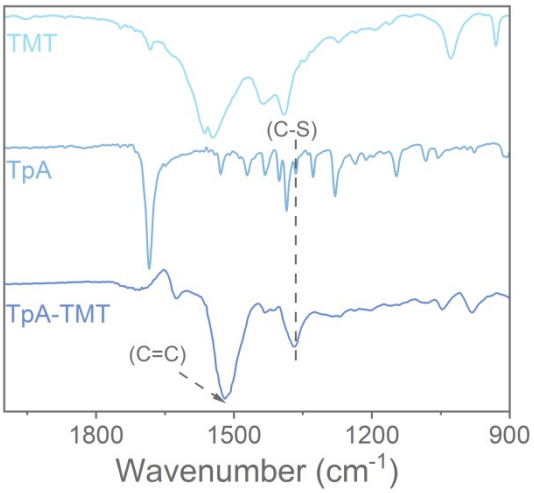

Figure S4. FTIR spectra of TpA-TMT.

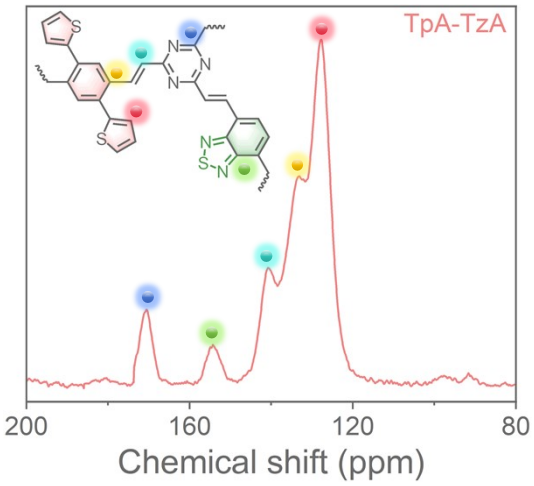

Figure S5. ^{13}C CP/MAS NMR spectra of TpA-TzA.

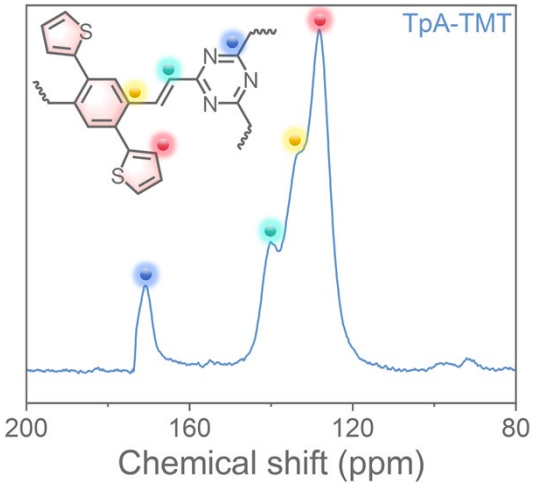

Figure S6. ^{13}C CP/MAS NMR spectra of TpA-TMT.

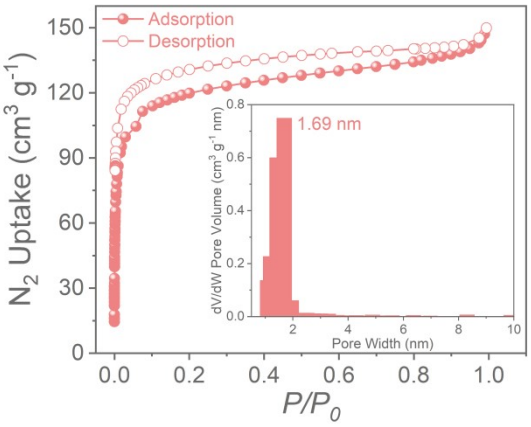

Figure S7. N_2 adsorption/desorption isotherms of TpA-TzA.

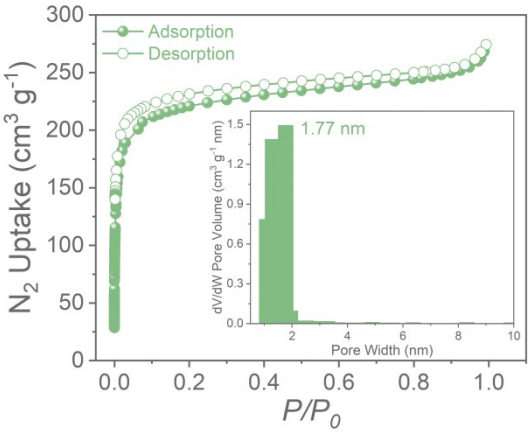

Figure S8. N_2 adsorption/desorption isotherms of TzA-TMT.

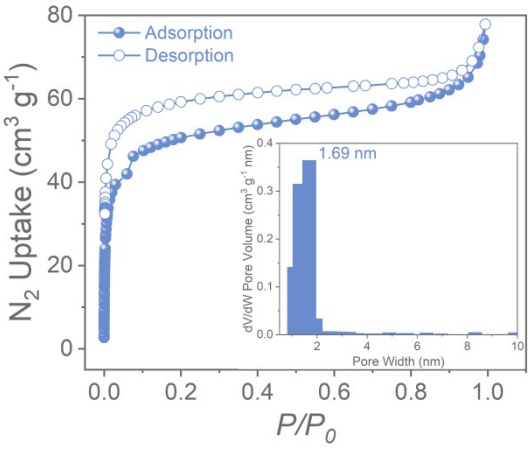

Figure S9. N_2 adsorption/desorption isotherms of TpA-TMT.

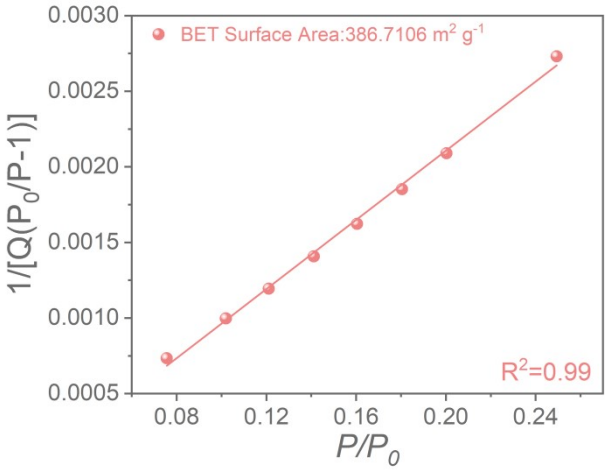

Figure S10. BET surface area plots of TpA-TzA calculated from the isotherms.

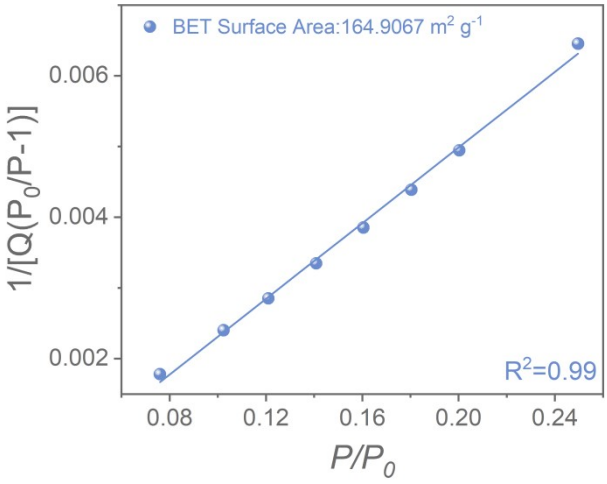

Figure S11. BET surface area plots of TpA-TMT calculated from the isotherms.

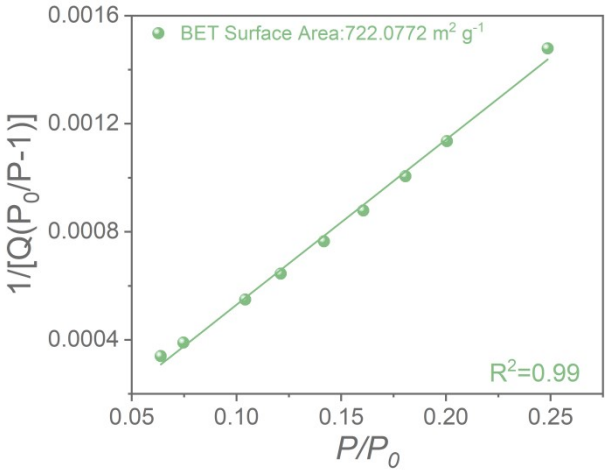

Figure S12. BET surface area plots of TzA-TMT calculated from the isotherms.

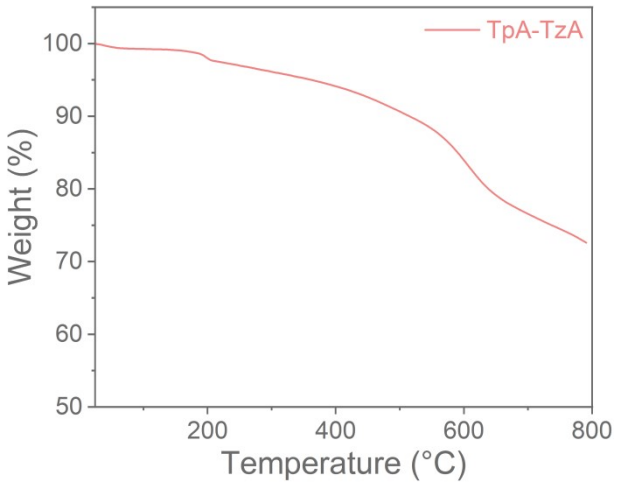

Figure S13. TGA curve of TpA–TzA.

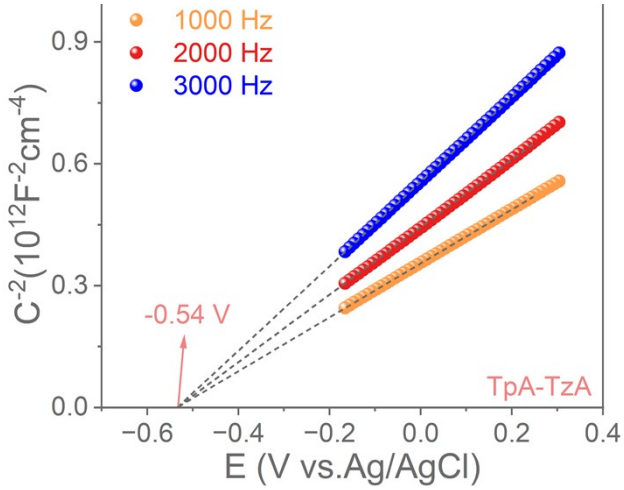

Figure S14. Mott-Schottky plots of TpA-TzA.

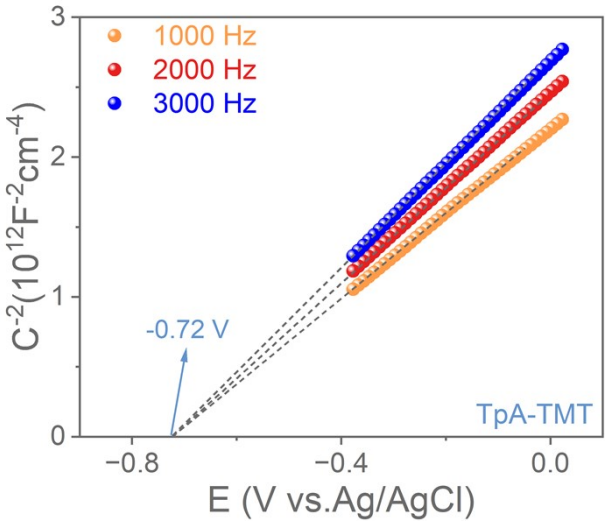

Figure S15. Mott-Schottky plots of TpA-TMT.

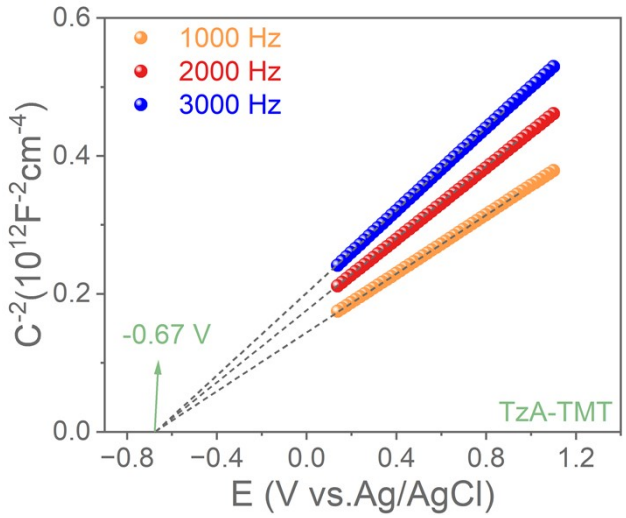

Figure S16. Mott-Schottky plots of TzA-TMT.

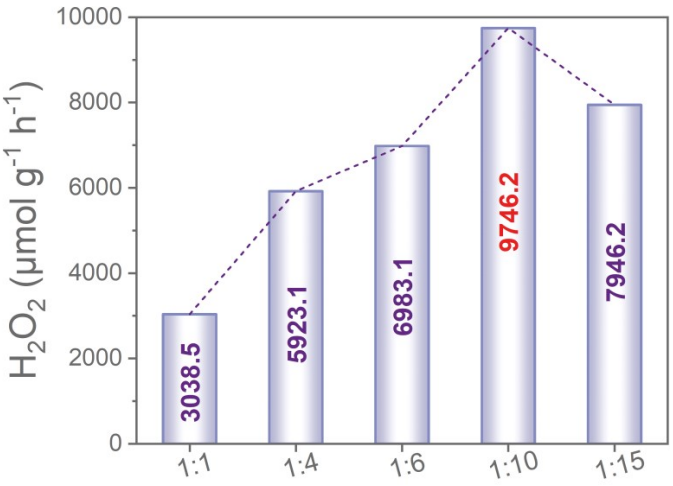

Figure S17. H_2O_2 production rates at various concentrations of TpA-TzA.

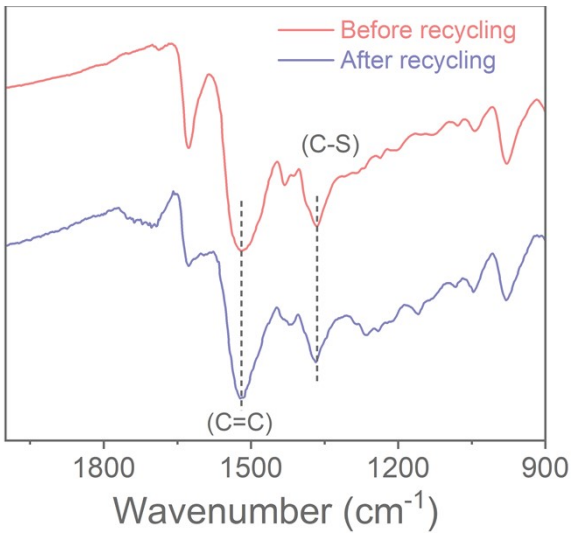

Figure S18. FI-IR of TpA-TzA before and after recycling experiments.

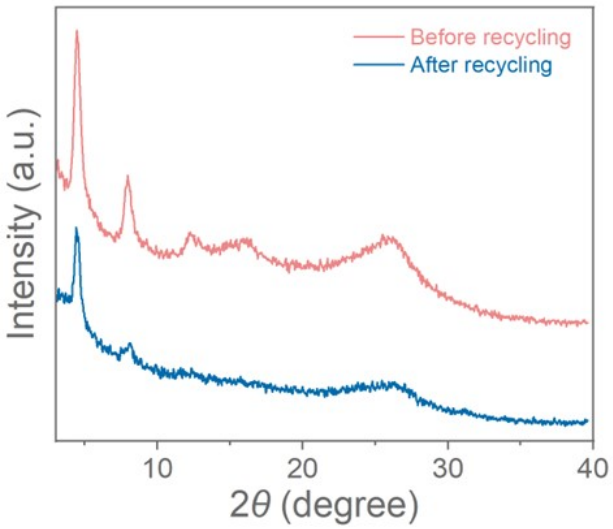

Figure S19. PXRD patterns of TpA-TzA before and after recycling experiments.

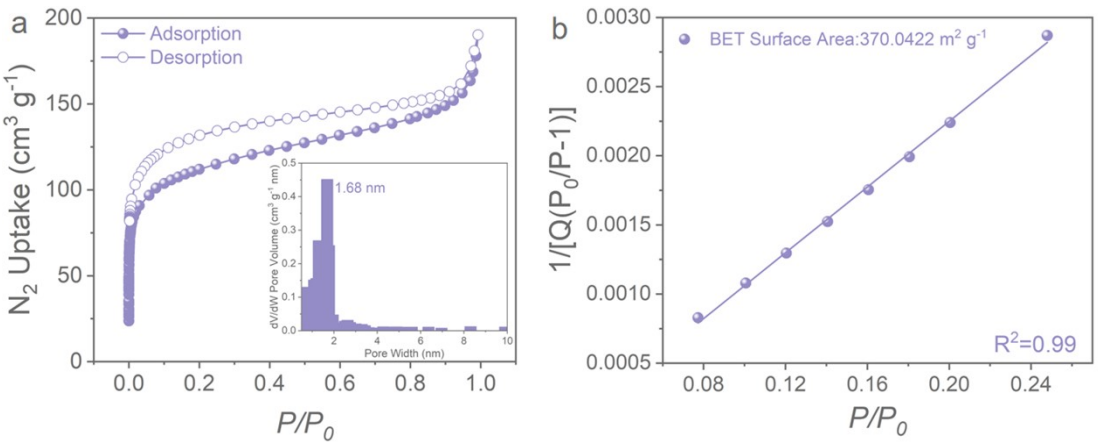

Figure S20. a N_2 adsorption/desorption isotherms of TpA-TzA after catalytic cycling. b BET surface area of TpA–TzA calculated from the isotherms following recycling experiments.

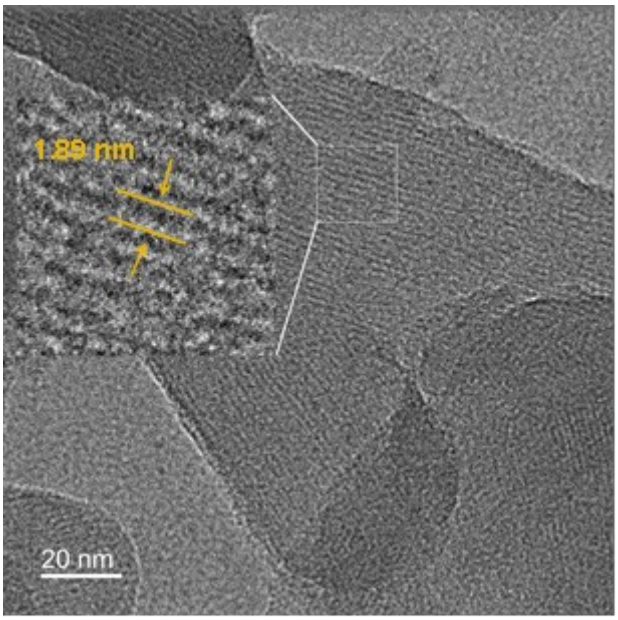

Figure S21. TEM image of TpA-TzA after recycling experiments.

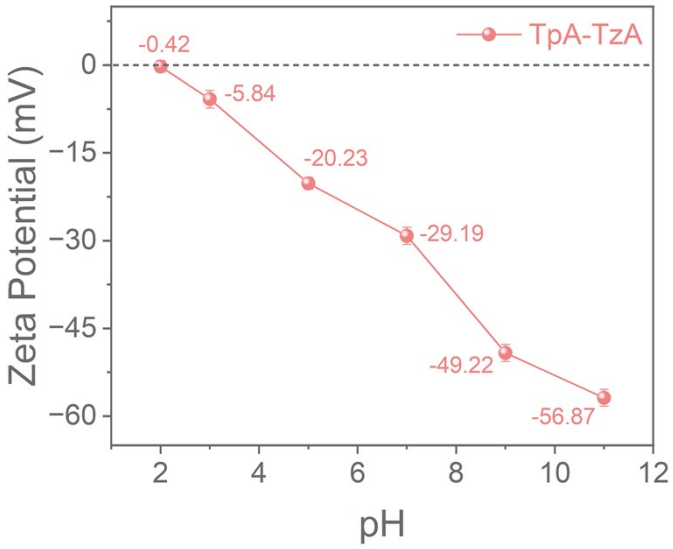

Figure S22. Zeta potential of TpA-TzA as a function of pH.

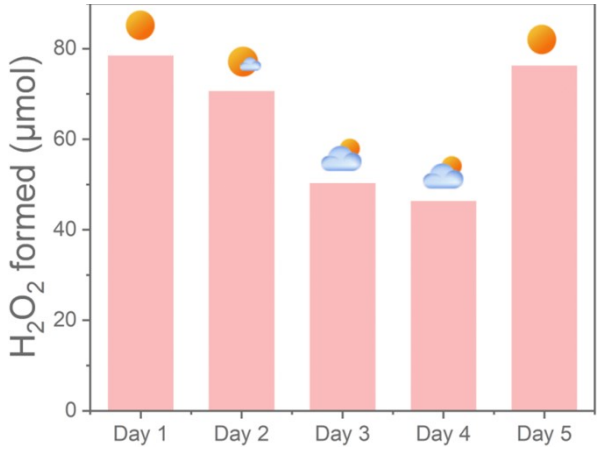

Figure S23. Photocatalytic H_2O_2 evolution by TpA-TzA under sunlight by using pure water in 2025.

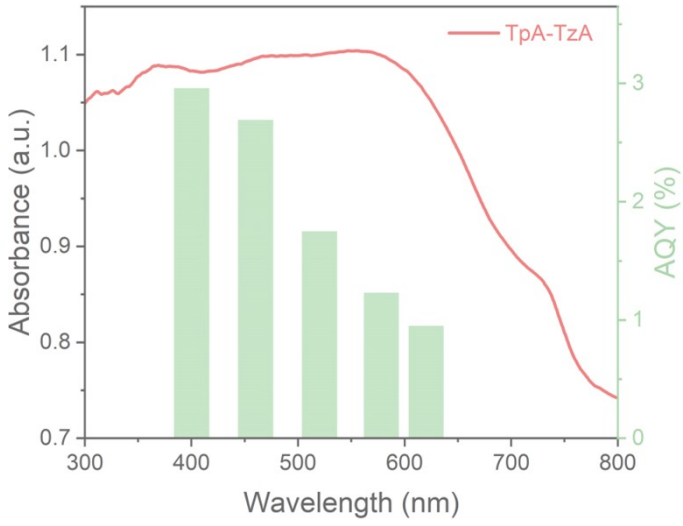

Figure S24. AQY of TpA-TzA.

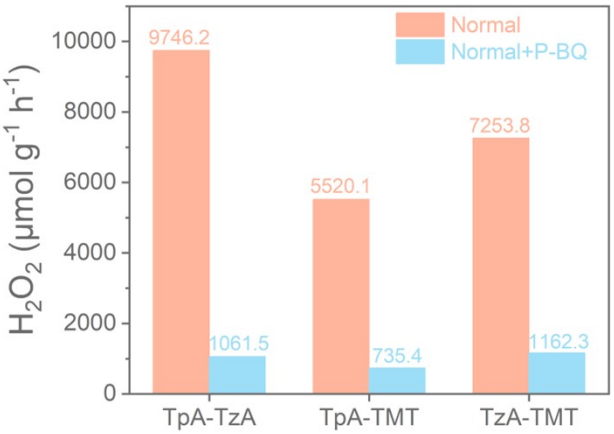

Figure S25. H_2O_2 production rates of TpA-TzA, TpA-TMT and TzA-TMT in the presence of *p*-BQ scavenger.

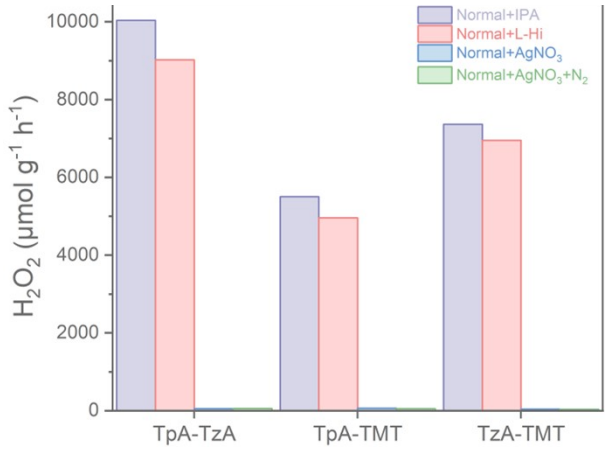

Figure S26. H_2O_2 production rates of TpA-TzA, TpA-TMT and TzA-TMT in the presence of IPA, L-hi, $AgNO_3$, $AgNO_3$+N_2 scavenger.

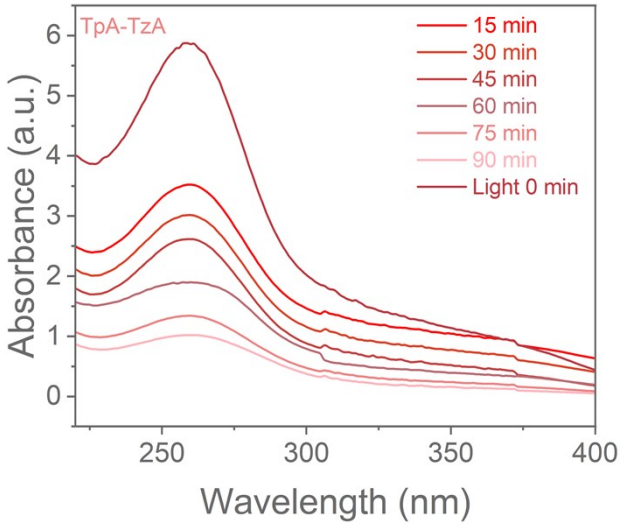

Figure S27. Detecting $\cdot O_2^-$ in TpA-TzA photocatalytic systems by NBT.

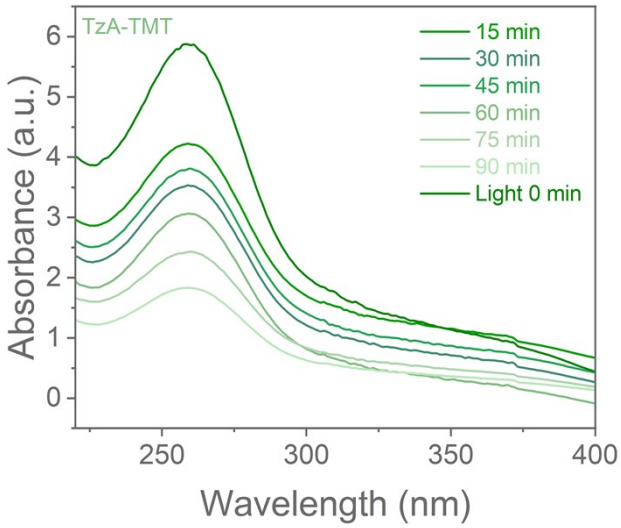

Figure S28. Detecting $\cdot O_2^-$ in TzA-TMT photocatalytic systems by NBT.

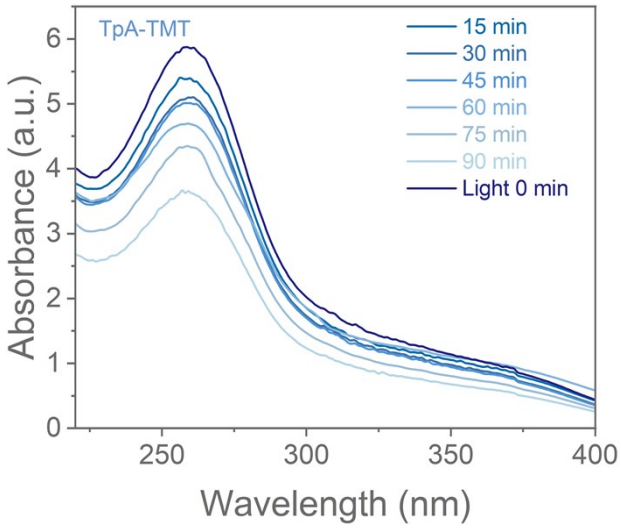

Figure S29. Detecting $\cdot O_2^-$ in TpA-TMT photocatalytic systems by NBT.

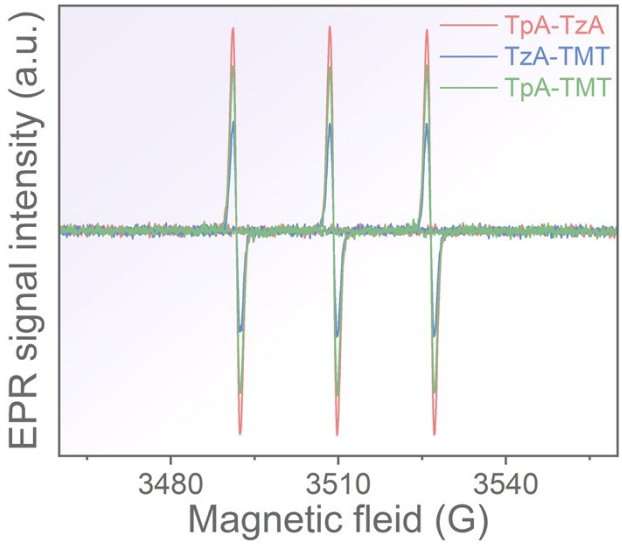

Figure S30. EPR signals by $^1O_2$ of TpA-TzA, TpA-TMT and TzA-TMT.

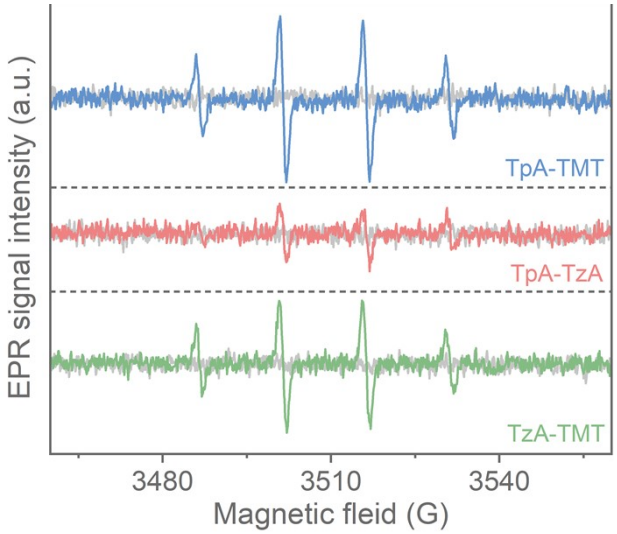

Figure S31. EPR signals by ·OH of TpA-TzA, TpA-TMT and TzA-TMT.

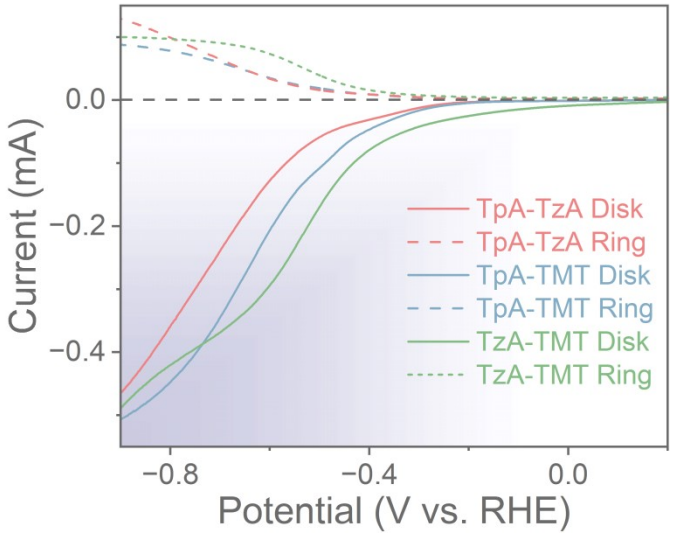

Figure S32. RRDE polarization curves over TpA-TzA, TpA-TMT and TzA-TMT in an O_2-saturated PBS solution (0.1 M) at 1600 rpm with ring current (top) and disk current (bottom).

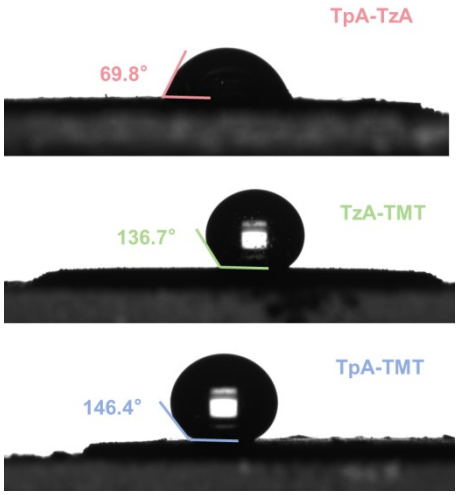

Figure S33. Water contact angles of TpA-TzA, TpA-TMT and TzA-TMT.

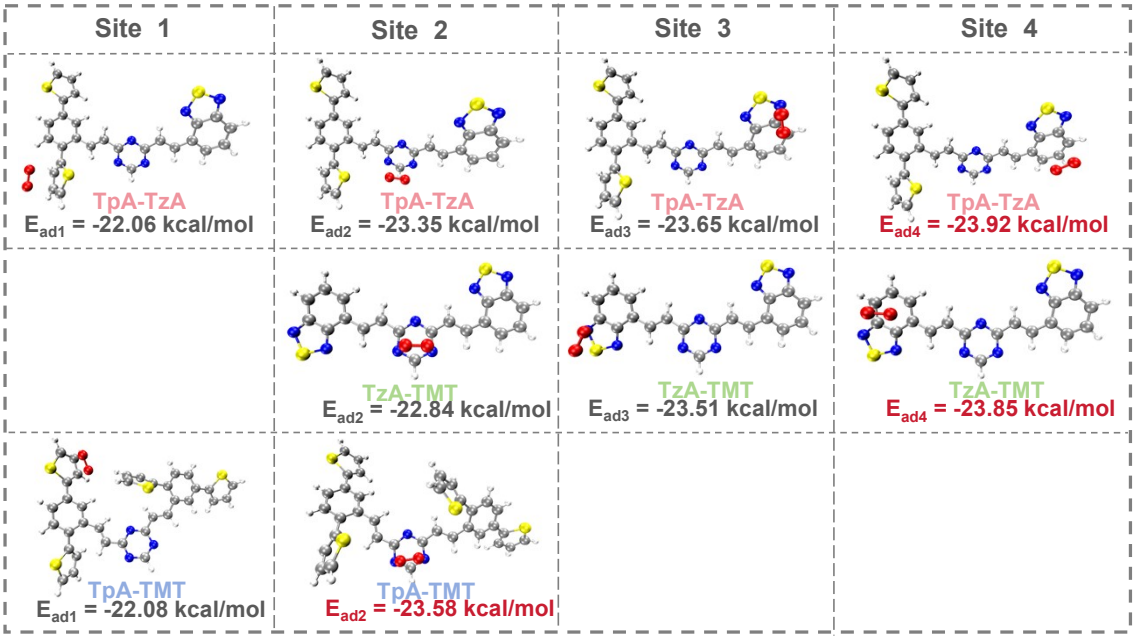

Figure S34. Different O_2 adsorption configurations and adsorption energy for TpA-TzA, TpA-TMT and TzA-TMT.

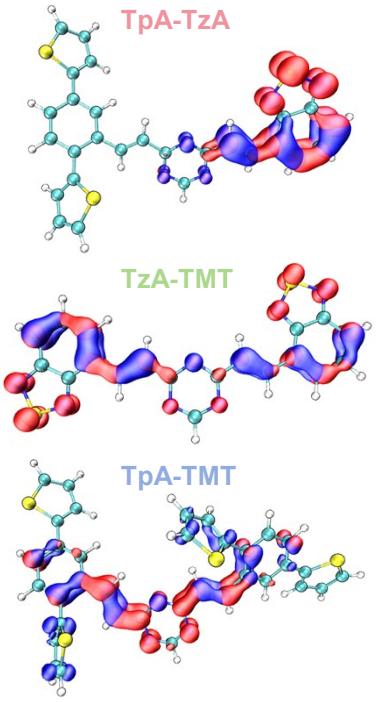

Figure S35. Charge density difference between the ground state and excited state for TpA-TzA, TzA-TMT and TpA-TMT.

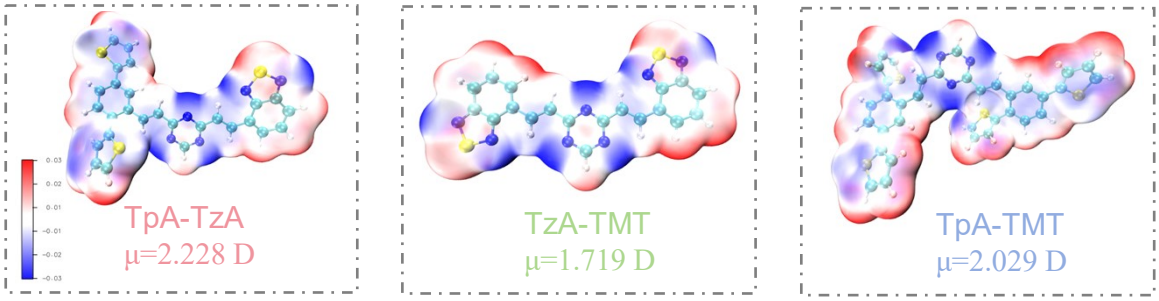

Figure S36. Electrostatic potential surfaces for TpA-TzA, TzA-TMT and TpA-TMT.

Table S1. Synthesis of the TpA-TzA under variable conditions.

Conditions	**Ratio**	**Temperature**	**Catalyst**	**Product**
n-BuOH/*o*-DCB	7/3	120 °C	KOH	Hight
n-BuOH/*o*-DCB	7/3	120 °C	trifluoroacetic	Poor
n-BuOH/*o*-DCB	7/3	120 °C	EtONa	Poor
n-BuOH/*o*-DCB	7/3	120 °C	DBU	Amorphous

n-BuOH/*o*-DCB	7/3	120 °C	TEB	Amorphous
n-BuOH/*o*-DCB	7/3	120 °C	Pyridine	Amorphous
n-BuOH/*o*-DCB	1:1	120 °C	KOH	Poor
o-DCB	1	120 °C	KOH	Amorphous
n-BuOH	1	120 °C	KOH	Amorphous
n-BuOH/*o*-DCB	3/7	120 °C	KOH	Amorphous

Table S2. Fractional atomic coordinates for the unit cell of TpA-TzA after Pawley refinement.

TpA-TzA in eclipsed model			
TpA-TzA:Space group symmetry			
***a*=22.8943 Å, *b*=3.5142 Å, *c*=22.8543 Å, *α*=*γ*=90.0000° *β*=60.1248°**			
Atom	**x/a**	**y/b**	**z/c**
N1	0.77755	-0.50000	-0.60409
C2	0.82316	-0.50000	-0.58305
N3	0.80182	-0.50000	-0.51612
C4	0.73513	-0.50000	-0.47052
N5	0.68962	-0.50000	-0.49207
C6	0.71072	-0.50000	-0.55890
C7	0.66074	-0.50000	-0.58173
C8	0.89514	-0.50000	-0.63376
C9	0.67942	-0.50000	-0.64799
C10	0.94387	-0.50000	-0.61736
N11	0.39817	-0.50000	0.19611
C12	0.35432	-0.50000	0.17272
N13	0.37790	-0.50000	0.10532
C14	0.44498	-0.50000	0.06152
N15	0.48861	-0.50000	0.08532
C16	0.46546	-0.50000	0.15252
C17	0.46943	-0.50000	-0.01144
C18	0.51416	-0.50000	0.17694
C19	0.28159	-0.50000	0.22121
C20	0.53534	-0.50000	-0.05760
C21	0.56315	-0.50000	-0.13201
C22	0.49479	-0.50000	0.24336
C23	0.53910	-0.50000	0.27468
C24	0.23510	-0.50000	0.20174
C25	0.16094	-0.50000	0.24864
C26	0.63325	-0.50000	-0.17524
C27	0.66188	-0.50000	-0.24408
C28	0.62215	-0.50000	-0.27558
C29	0.55167	-0.50000	-0.23293

C30	0.52245	-0.50000	-0.16236
C31	0.11710	-0.50000	0.22229
C32	0.04846	-0.50000	0.26289
C33	0.01783	-0.50000	0.33405
C34	0.06109	-0.50000	0.36134
C35	0.13142	-0.50000	0.31959
C36	0.51470	-0.50000	0.34613
C37	0.56476	-0.50000	0.36532
C38	0.63505	-0.50000	0.32096
C39	0.65954	-0.50000	0.24954
C40	0.60948	-0.50000	0.23037
C41	0.64829	-0.50000	-0.34986
C42	0.71347	-0.50000	-0.39821
C43	0.44116	-0.50000	0.40544
C44	0.73323	-0.50000	0.19027
S45	0.74974	-0.50000	0.10721
C46	0.83386	-0.50000	0.07691
C47	0.85041	-0.50000	0.12639
C48	0.79489	-0.50000	0.18981
C49	0.37963	-0.50000	0.40578
C50	0.32410	-0.50000	0.46916
C51	0.34056	-0.50000	0.51870
S52	0.42465	-0.50000	0.48853
N53	0.01639	-0.50000	0.22725
S54	0.07041	-0.50000	0.14307
N55	0.13684	-0.50000	0.15626
N56	0.72937	-0.50000	-0.27547
S57	0.75856	-0.50000	-0.22051
N58	0.67886	-0.50000	-0.15466
H59	0.60925	-0.50000	-0.54149
H60	0.90588	-0.50000	-0.68516
H61	0.73131	-0.50000	-0.67956
H62	0.92856	-0.50000	-0.56414
H63	0.43126	-0.50000	-0.02589
H64	0.56581	-0.50000	0.13708
H65	0.26757	-0.50000	0.27372
H66	0.57143	-0.50000	-0.03986
H67	0.44272	-0.50000	0.27439

Table S3. Fractional atomic coordinates for the unit cell of TpA-TMT after Pawley refinement.

TpA-TMT in eclipsed model			
TpA-TMT:Space group symmetry			
***a*=22.9965 Å, *b*=3.5135 Å, *c*=22.9956Å, *α*=*γ*=90.0000° *β*=120.0161°**			
Atom	**x/a**	**y/b**	**z/c**
N1	0.20142	0.50000	0.81522
C2	0.26894	0.50000	0.85607
N3	0.30880	0.50000	0.82867
C4	0.28211	0.50000	0.76115

N5	0.21483	0.50000	0.72127
C6	0.17401	0.50000	0.74795
C7	0.10087	0.50000	0.70160
C8	0.29573	0.50000	0.92921
C9	0.04982	0.50000	0.71463
C10	0.35981	0.50000	0.98031
N11	0.61526	0.50000	0.42831
C12	0.54774	0.50000	0.38746
N13	0.50788	0.50000	0.41486
C14	0.53458	0.50000	0.48238
N15	0.60185	0.50000	0.52226
C16	0.64267	0.50000	0.49558
C17	0.48823	0.50000	0.50915
C18	0.71581	0.50000	0.54193
C19	0.52095	0.50000	0.31432
C20	0.50124	0.50000	0.57323
C21	0.44782	0.50000	0.59153
C22	0.76686	0.50000	0.52890
C23	0.83861	0.50000	0.58230
C24	0.45687	0.50000	0.26322
C25	0.43857	0.50000	0.19149
C26	0.47689	0.50000	0.66119
C27	0.43903	0.50000	0.69347
C28	0.36886	0.50000	0.65199
C29	0.33979	0.50000	0.58234
C30	0.37765	0.50000	0.55006
C31	0.36892	0.50000	0.15088
C32	0.33664	0.50000	0.08072
C33	0.37811	0.50000	0.05204
C34	0.44776	0.50000	0.09265
C35	0.48004	0.50000	0.16281
C36	0.87916	0.50000	0.55321
C37	0.94932	0.50000	0.59105
C38	0.97807	0.50000	0.66123
C39	0.93752	0.50000	0.69032
C40	0.86736	0.50000	0.65248
C41	0.54870	0.50000	0.68939
C42	0.26799	0.50000	0.55414
C43	0.31544	0.50000	0.67030
C44	0.32846	0.50000	0.73438
C45	0.83551	0.50000	0.48140
C46	0.98118	0.50000	0.76212
C47	0.34072	0.50000	0.19446
C48	0.47596	0.50000	0.04906
S49	0.96571	0.50000	0.82691
C50	1.05163	0.50000	0.87867
C51	1.08855	0.50000	0.84585
C52	1.04629	0.50000	0.77754
S53	0.20322	0.50000	0.47385
C54	0.15144	0.50000	0.50797
C55	0.18425	0.50000	0.57773
C56	0.25256	0.50000	0.60382
C57	0.56413	0.50000	0.63971
C58	0.63243	0.50000	0.66580

C59	0.66524	0.50000	0.73556
S60	0.61347	0.50000	0.76968
C61	0.39040	0.50000	0.25960
C62	0.36432	0.50000	0.30181
C63	0.29456	0.50000	0.26483
S64	0.26044	0.50000	0.17892
S65	0.55624	0.50000	0.06461
C66	0.52213	0.50000	-0.02130
C67	0.45237	0.50000	-0.05828

Table S4. Fractional atomic coordinates for the unit cell of TzA-TMT after Pawley refinement.

TzA-TMT in eclipsed model			
TzA-TMT:Space group symmetry			
***a*=22.8740 Å, *b*=3.5122 Å, *c*=22.8739Å, *α*=*γ*=90.0000° *β*=60.0007°**			
Atom	**x/a**	**y/b**	**z/c**
N1	0.80705	-0.50000	-0.63797
C2	0.85323	-0.50000	-0.61750
N3	0.83234	-0.50000	-0.55065
C4	0.76569	-0.50000	-0.50448
N5	0.71974	-0.50000	-0.52537
C6	0.74021	-0.50000	-0.59202
C7	0.68925	-0.50000	-0.61327
C8	0.92543	-0.50000	-0.66846
C9	0.70581	-0.50000	-0.67852
C10	0.97413	-0.50000	-0.65190
N11	0.42962	-0.50000	0.16253
C12	0.38564	-0.50000	0.13931
N13	0.40926	-0.50000	0.07191
C14	0.47647	-0.50000	0.02793
N15	0.52024	-0.50000	0.05155
C16	0.49702	-0.50000	0.11876
C17	0.50082	-0.50000	-0.04500
C18	0.54559	-0.50000	0.14311
C19	0.31271	-0.50000	0.18789
C20	0.56680	-0.50000	-0.09142
C21	0.59447	-0.50000	-0.16579
C22	0.52603	-0.50000	0.20910
C23	0.57273	-0.50000	0.23677
C24	0.26629	-0.50000	0.16832
C25	0.19191	-0.50000	0.21502
C26	0.66468	-0.50000	-0.20933
C27	0.69319	-0.50000	-0.27817
C28	0.65321	-0.50000	-0.30935
C29	0.58260	-0.50000	-0.26639
C30	0.55352	-0.50000	-0.19583
C31	0.14837	-0.50000	0.18835
C32	0.07954	-0.50000	0.22868
C33	0.04836	-0.50000	0.29985

C34	0.09132	-0.50000	0.32749
C35	0.16188	-0.50000	0.28602
C36	0.54606	-0.50000	0.30698
C37	0.58639	-0.50000	0.33549
C38	0.65756	-0.50000	0.29550
C39	0.68520	-0.50000	0.22489
C40	0.64372	-0.50000	0.19581
C41	0.67919	-0.50000	-0.38358
C42	0.74444	-0.50000	-0.43227
N43	0.04782	-0.50000	0.19277
S44	0.10247	-0.50000	0.10863
N45	0.16864	-0.50000	0.12224
N46	0.76082	-0.50000	-0.30988
S47	0.79031	-0.50000	-0.25523
N48	0.71053	-0.50000	-0.18907
N49	0.55048	-0.50000	0.40311
S50	0.46634	-0.50000	0.43261
N51	0.47995	-0.50000	0.35283
H52	0.63777	-0.50000	-0.57275
H53	0.93639	-0.50000	-0.71994
H54	0.75908	-0.50000	-0.71623
H55	0.95857	-0.50000	-0.59863
H56	0.46246	-0.50000	-0.05920
H57	0.59816	-0.50000	0.10475
H58	0.29851	-0.50000	0.24045
H59	0.60306	-0.50000	-0.07392
H60	0.47227	-0.50000	0.24536
H61	0.28378	-0.50000	0.11456
H62	0.54940	-0.50000	-0.28749
H63	0.49912	-0.50000	-0.16588
H64	0.07023	-0.50000	0.38179
H65	0.19184	-0.50000	0.31046
H66	0.73950	-0.50000	0.19169
H67	0.66817	-0.50000	0.14141

Table S5. Comparison of the photocatalytic H_2O_2 production rate over representative metal-free photocatalysts for sacrificial agent-free H_2O_2 photosynthesis.

	Photocatalyst	**Temp. (ºC)**	**SCC% Conc. (g L^{-1})**	**AQY**	**H_2O_2 production (μmol h^{-1} g^{-1})**	**Ref.**
This works	**TpA-TzA**	**25**	**0.25**	**2.96@420nm**	**9746.2**	**This works**
	TzA-TMT	**25**	**-**	**-**	**7253.8**	**This works**
	TpA-TMT	**25**	**-**	**-**	**5520.1**	**This works**

COFs	TpaBtt-	25	0.296	4.6@450nm	1407	[1]
	TPB-	r.t.	0.76	18.4@420nm	1550	[2]
	COF-2CN	25	0.6	6.8@459nm	1601	[3]
	COF-	-	0.65	8.6@420nm	2084	[4]
	TTF-BT-	25	0.49	11.19@420nm	2760	[5]
	TD-COF	-	0.15	-	3364	[6]
	Byp-TAPT	-	0.65	8.6@420nm	4038	[7]
	Hz-TP-BT-	r.t.	-	17.5@420nm	5700	[8]
	Pylm-COF	-	0.28	3.70@420nm	5850	[9]
	TAH-COF	-	0.66	7.72@500nm	6003	[10]
	TpDZ	-	0.62	11.9@420nm	7327	[11]
	TBTN-	-	-	7.59@420nm	11013	[12]
	CTF-BP	25	-	3.1@420nm	426.1	[13]
	CQD-CT	-	-	1.03@420nm	535.41	[14]
	THTB-Py-	-	-	9.32@450nm	4200	[15]
	TTA-Azo-	-	0.64	8.2@500nm	2516	[16]
CTFs	CTF-FL	25	-	8.6@420nm	2412.1	[13]
	Bpt-CTF	-	0.20	8.6@400nm	3268.1	[17]
	TTH-CTP	25	-	11.3@450nm	4100	[18]
	CTF-NSs	25	0.91	16.8@420nm	5007	[13]
CMPs	DE7-M	-	0.28	8.7@420nm	1200	[19]
	AQTEE-	-	-	3.59@400nm	3204	[20]
	BBTz	-	-	2.60@475nm	7274	[21]
S/Z-Scheme	CT-10	25	-	-	1036.9	[22]
	TB-6	-	-	5.48@420nm	1480	[23]
	ZT-5	-	-	13.12@365nm	2440	[24]
	CdS/TpBp	-	-	13.4@380nm	3600	[25]
	BIT6	-	0.91	6.50@420nm	5788	[26]

References

[1] C. Qin, X. Wu, L. Tang, X. Chen, M. Li, Y. Mou, B. Su, S. Wang, C. Feng, J. Liu, X. Yuan, Y. Zhao and H. Wang, *Nat. Commun*, 2023, 14, 5238.

[2] L. Li, L. Xu, Z. Hu and J.C. Yu, *Adv. Funct. Mater*, 2021, 31, 2106120.

[3] Y. Hou, P. Zhou, F. Liu, Y. Lu, H. Tan, Z. Li, M. Tong and J. Ni, *Adv. Funct. Mater*, 2024, 63, e202318562.

[4] M. Kou, Y. Wang, Y. Xu, L. Ye, Y. Huang, B. Jia, H. Li, J. Ren, Y. Deng, J. Chen, Y. Zhou, K. Lei, L. Wang, W. Liu, H. Huang and T. Ma, *Adv. Funct. Mater*, 2022, 61, e202200413.

[5] J.-N. Chang, Q. Li, J.-W. Shi, M. Zhang, L. Zhang, S. Li, Y. Chen, S.-L. Li and Y.-Q. *Angew. Chem. Int. Ed*, 2023, 62, e202218868.

[6] J.-Y. Yue, L.-P. Song, Y.-F. Fan, Z.-X. Pan, P. Yang, Y. Ma, Q. Xu and B. Tang, *Angew. Chem. Int. Ed*, 2023, 135, e202309624.

[7] Y. Liu, W.-K. Han, W. Chi, Y. Mao, Y. Jiang, X. Yan and Z.-G. Gu, *App. Catal. B: Environ*, 2023, 331, 22691.

[8] R. Liu, Y. Chen, H. Yu, M. Položij, Y. Guo, T.C. Sum, T. Heine and D. Jiang, *Nat. Catalysis*, 2024, 7, 195-206.

[9] W. Wu, Z. Li, S. Liu, D. Zhang, B. Cai, Y. Liang, M. Wu, Y. Liao and X. Zhao, *Angew. Chem. Int. Ed*, 2024, 63, e202404563.

[10] T. Xu, Z. Wang, W. Zhang, S. An, L. Wei, S. Guo, Y. Huang, S. Jiang, M. Zhu, Y.-B. Zhang and W.-H. Zhu, *J. Am. Chem. Soc*, 2024, 146, 20107-20115.

[11] Q. Liao, Q. Sun, H. Xu, Y. Wang, Y. Xu, Z. Li, J. Hu, D. Wang, H. Li and K. Xi, *Angew. Chem. Int. Ed*, 2023, 62, e202310556.

[12] E. Zhou, F. Wang, X. Zhang, Y. Hui and Y. Wang, *Angew. Chem. Int. Ed*, 2024, 63, e202400999.

[13] L. Zhang, C. Wang, Q. Jiang, P. Lyu and Y. Xu, *J. Am. Chem. Soc*, 2024, 146, 29943-29954.

[14] Y. Yang, Q. Guo, Q. Li, L. Guo, H. Chu, L. Liao, X. Wang, Z. Li and W. Zhou, *Adv. Funct. Mater*, 2024, 34, 2400612.

[15] J.-X. Li, Z.-H. Zhao, Y.-X. Jiang, C.-Y. Jing, H.-T. Che, G.-Y. Zhang, Y. Wang, H. Dong and F.-M. Zhang, *Appl. Catal. B: Environ. Energy*, 2026, 383, 126013.

[16] J.-Z. Xiao, Z.-H. Zhao, N.-N. Zhang, H.-T. Che, X. Qiao, G.-Y. Zhang, X. Chu, Y. Wang, H. Dong and F.-M. Zhang, *Chin. J. Catal.*, 2025, 69, 219-229.

[17] C. Wu, Z. Teng, C. Yang, F. Chen, H.B. Yang, L. Wang, H. Xu, B. Liu, G. Zheng and Q. Han, *Adv. Mater*, 2022, 34, 2110266.

[18] S. Wang, Z. Xie, D. Zhu, S. Fu, Y. Wu, H. Yu, C. Lu, P. Zhou, M. Bonn, H.I. Wang, Q. Liao, H. Xu, X. Chen and C. Gu, *Nat. Commun*, 2023, 14, 6891.

[19] B. He, Z. Wang, P. Xiao, T. Chen, J. Yu and L. Zhang, *J. Am. Chem. Soc*, 2022, 34, 2203225.

[20] X. Xu, R. Sa, W. Huang, Y. Sui, W. Chen, G. Zhou, X. Li, Y. Li and H. Zhong, *ACS Catal*, 2022, 12, 12954-12963.

[21] J. Cheng, S. Wan and S. Cao, *Angew. Chem. Int. Ed*, 2023, 62, e202310476.

[22] Y. He, J. Zhao, Y.-T. Sham, S. Gao, M. Pan, Q. Chen, G. Huang, P.K. Wong and J. Bi, *ACS Sustainable Chem. Eng*, 2023, 11, 17552-17563.

[23] Y. Yang, J. Liu, M. Gu, B. Cheng, L. Wang and J. Yu, *Appl. Catal. B Environ*, 2023, 333, 122780.

[24] Y. Zhang, J. Qiu, B. Zhu, M.V. Fedin, B. Cheng, J. Yu and L. Zhang, *Chem. Eng. J*, 2022, 444, 136584.

[25] X. Li, D. Chen, N. Li, Q. Xu, H. Li and J. Lu, *J. Colloid Interf. Sci*, 2023, 648, 664-673.

[26] J.-Y. Yue, Z.-X. Pan, P. Yang and B. Tang, *ACS Mater. Letters*, 2024, 6, 3932-3940.